Impact of spin-entropy on the thermoelectric properties of a 2D magnet

Supplementary Information

Alessandra Canetta,[†] Serhii Volosheniuk,[‡] Sayooj Satheesh,[¶] José Pedro Alvarinhas Batista,[§] Aloïs Castellano,[§] Riccardo Conte,[‡] Daniel George Chica,[‖] Kenji Watanabe,[⊥] Takashi Taniguchi,[#] Xavier Roy,[‖] Herre S.J. van der Zant,[‡] Marko Burghard,[¶] Matthieu Jean Verstraete,[§,@] and Pascal Gehring[*,†]

†*Institute of Condensed Matter and Nanosciences, Université catholique de Louvain (UCLouvain), 1348 Louvain-la-Neuve, Belgium*

‡*Kavli Institute of Nanoscience, Delft University of Technology, 2628CJ Delft, The Netherlands*

¶*Max-Planck-Institut für Festkörperforschung, D-70569 Stuttgart, Germany*

§*Nanomat/Q-MAT/CESAM and European Theoretical Spectroscopy Facility, Université de Liège, B-4000, Liège, Belgium*

‖*Department of Chemistry, Columbia University, New York, NY, 10027 USA*

⊥*Research Center for Electronic and Optical Materials, National Institute for Materials Science, 1-1 Namiki, Tsukuba 305-0044, Japan*

#*Research Center for Materials Nanoarchitectonics, National Institute for Materials Science, 1-1 Namiki, Tsukuba 305-0044, Japan*

@*ITP, Physics Department Utrecht University 3508 TA Utrecht, The Netherlands*

E-mail: pascal.gehring@uclouvain.be

Contents

1 Synthesis and exfoliation of CrSBr flakes

Crystals of CrSBr were synthesized using a chemical vapor transport method. This synthetic technique involved the transport of material from 950 °C at the source side to 850 °C at the sink side of a slightly off stoichiometric combination of Cr, S, and $CrBr_3$ in an evacuated fused silica ampoule. The detailed synthesis and cleaning procedure can be found elsewhere.[1] Exfoliation of CrSBr flakes is performed directly on a polydimethylsiloxane (PDMS) square of approximately 1 mm x 1 mm positioned on a glass slide. This is a well-known methodology to transfer 2D materials and a complete description can be found elsewhere.[2,3] The PDMS surface is cleaned by bringing some fresh tape in contact with it and peeling it off as quickly as possible. CrSBr flakes are then mechanically exfoliated on the PDMS square using the Scotch tape method.[4,5] Thin flakes are then selected via optical contrast. In order to avoid contamination and air degradation, exposed CrSBr flakes are constantly handled under inert atmosphere in a N_2 glove box, with $<$0.5 ppm of O_2 and $<$0.5 ppm of H_2O content.

2 Atomic Force Microscopy measurements

The thickness of each flake, firstly identified by optical contrast, is confirmed by means of Atomic Force Microscopy. Topography maps are measured in tapping mode in a Bruker Dimension Icon system. Results are then analyzed on the software Gwyddion. Thickness values (t) of the flake are extracted as the height difference with respect to the substrate level, considered as reference level and therefore set as zero (see Fig. S1). Fig. S1 displays the topography map of the CrSBr flake studied in the main text. Its thickness is found to be equal to 6.2 nm, corresponding to 8 layers.

3 Evaluation of the electrical conductivity

Flake lenght (l) and width (w) are easily evaluated via optical microscopy and respectively equal to 5 µm and 2.5 µm. Once these three parameters are known, it is possible to calculate the electrical

conductivity σ of the device from its resistance values by applying the following formula:

$$\sigma = \frac{1}{R} \cdot \frac{l}{t \cdot w} \tag{1}$$

The temperature-dependent electrical conductivity of the device is reported in Fig. S2. Such values are then used to evaluate the temperature-dependent power factor as $PF = \alpha^2 \cdot \sigma$.

4 Pre-patterned thermopower contacts

Thermopower contacts are defined by standard Electron Beam Lithography (EBL) on a Silicon (Si) wafer with a 285 nm top layer of Silicon Oxide (SiO_2). First, the heaters are fabricated by depositing 3 nm of Titanium (Ti) and 27 nm of Palladium (Pd). Afterwards, the sample is covered by 10 nm of Aluminum Oxide (Al_2O_3) via atomic layer deposition (ALD), performed in an Oxford Instruments FlexAL system. Finally, 3 nm of Ti and 47 nm of Gold (Au) are deposited as top contacts.

5 CrSBr device fabrication

CrSBr selected flakes are stamped on top of the golden contacts by means of a home-built 2D materials transfer system controlled via Thorlabs Kinesis software. The PDMS stamp is positioned on top of the contacts, making sure that the chosen flake is bridging between the two golden resistors. Thus, the glass slide is lowered and the CrSBr flake is brought in contact with the sample surface, on which it adheres. The PDMS stamp is then slowly lifted in order to let the flake stick to the surface.[2,3] No heat sources are used in the context of this process. In order to preserve CrSBr uncontaminated and to avoid air degradation, the flake is encapsulated with an hexagonal Boron Nitride (hBN) flake by means of a polypropylene carbonate (PPC)-PDMS stamp, according to the dry release transfer method described elsewhere.[6,7]

6 Thermoelectric and electrical transport measurements

Electrical transport and thermopower measurements are performed in a ^{4}He cryostat using home-built ultra-low noise voltage/current sources and pre-amplifiers. We employ a lock-in double-demodulation technique,[8] which allows to decouple the thermally induced electric current (thermocurrent) $\tilde{I}_{\mathrm{th}}$ flowing as a response to a thermal bias ΔT from $\tilde{I}_{\mathrm{sd}}$, the response to a voltage bias $\tilde{V}_{\mathrm{sd}}$.[8] To this end, an AC current $\tilde{I}_{\mathrm{h}} = 0.5$ mA (power $P = 0.12$ mW) at frequency $\omega_1 = 3$ Hz is applied to the Pd heater with a Stanford Research SR830 lock-in connected to a current source. Simultaneously, an AC voltage $\tilde{V}_{\mathrm{sd}} = 10$ mV at $\omega_2 = 13$ Hz is applied to the drain contact. The current at the source contact is pre-amplified by a low-noise transimpedance amplifier and demodulated at $2\omega_1$ and ω_2 to obtain $\tilde{I}_{\mathrm{th}}$ and $\tilde{I}_{\mathrm{sd}}$, respectively.

7 Field-dependent measurements of the thermoelectric properties of CrSBr

Additional thermoelectric measurements have been performed on other CrSBr flakes. The device shown in Fig. S3a consists in a 35 layer-thick non-encapsulated CrSBr flake. Thickness has been measured by means of Atomic Force Microscopy (see Fig. S3b) and evaluated as described in Section 2. In this case, the thermovoltage is extracted directly using the lock-in double-demodulation technique. The field dependence of the Seebeck coefficient, normalized with respect to the value at $B = 0$ T, is reported in Fig. S3d-e. The magnetic field is oriented along the a and b axis, respectively. The different shape of the curves represents the evidence for the strong anisotropy in CrSBr. In Fig. S3d the spins are canting as B is aligned with the medium axis a, while in Fig. S3e the field is applied along the easy axis b and therefore a spin-flip transition occurs.

8 Calibration of ΔT

In order to evaluate the Seebeck coefficient of CrSBr, it is necessary to know the temperature difference ΔT along the flake. Such parameter can be obtained by calibrating the temperature-dependent resistance of the two gold thermometers, defined as R_A and R_B. The setup used to calibrate thermometers A and B is displayed in Fig. S4a and b respectively. The calibration consists in a resistance measurement with and without a thermal gradient applied. Such gradient is generated via Joule effect, by feeding the heater on a current I_h. Fig. S5a-b shows the resistance values R_A and R_B, respectively, in a range between 20 K and 200 K. To perform the resistance measurement, both resistors are biased with a current of 1 μA. Let us consider the formula $R = R_0(1 + TCR(T - T_0))$, where TCR stands for Temperature Coefficient of Resistance. By linearly fitting the two curves, we extract the slopes in Fig. S5a-b, corresponding respectively to the products $TCR_A R_{0_A}$ = 0.045 Ω/K and $TCR_B R_{0_B}$ = 0.290 Ω/K. Fig. S5c-d report the resistance values on thermometers R_A and R_B, respectively, as a function of the power P produced on the heater. The AC current I_h is swept between 0 and 1.5 mA. The measurement is performed at a constant temperature of 30 K. Resistance values are then converted in temperature jumps δT induced by the thermal gradient on the two thermometers A and B, equal to 1.4 K and 0.1 K at 30 K. By subtracting the two temperature-dependent δT, we obtain the temperature difference ΔT at the extremes of the device at a given temperature. For the used power value of 0.12 mW we extract a ΔT of 1.3 $\pm$ 0.1 K at 30 K. By following this procedure, we are able to extract the values of ΔT for the temperatures in range between 20 and 220 K, therefore taking into account the temperature-dependent variation of ΔT.

9 Evaluation of the saturation field H_s

To extract the values of H_s reported in the main text (see Fig. 2f in the main text), a colormap of the second derivative of the MRR versus magnetic field and temperature, displayed in Fig. S6 was exploited. Here the saturation field values can be identified as the contour of the curve, where the second derivative tends to zero.[9]

10 Reactivity of CrSBr flakes

Despite CrSBr has been advertized as an air-stable material in many works,[10–12] recent studies, however, have proven that thin flakes of CrSBr undergo oxidation when exposed to ambient conditions.[13–15] A thorough study of the air instability of CrSBr flakes has been conducted by measuring the change in electrical resistance R of CrSBr flakes while initially keeping them in an inert atmosphere and thereafter exposing them to ambient conditions. To do so, two-terminal device geometries are patterned by EBL on a Si wafer with a 285 nm top layer of SiO_2. In order to exclude from the possible factors of degradation the mechanical strain on the flake edges, the contacts are almost completely buried in the oxide layer. To do so, an oxygen plasma descum process is performed on the sample, in order to ensure that there are no polymer traces - readily, the polymethyl methacrylate (PMMA) used in the previous lithography step - left on the exposed regions. Then, 40 nm of SiO_2 in the contact areas are etched by CHF_3 plasma via Reactive Ion Etching (RIE). The etched areas are then filled with 5 nm of Chromium (Cr) and 40 nm of Gold (Au) are deposited via e-beam evaporation. A CrSBr flake is then transferred on top of the pre-patterned structure via the dry transfer technique explained in Section 5. The device is then inserted in a home-made hermetically closed chamber equipped with a butterfly valve. The chamber is initially filled with N_2 and the resistance is recorded as a function of time ($t < 0$). At $t = 0$, the valve is open and the resistance is now measured while the flake is exposed to air (see Fig. S8a). Fig. S8b shows the resistance curves recorded for flakes with different thicknesses as a function of time t. A general increase of R has been detected in all the samples, ranging from a thickness of 6 nm to 27 nm. This study confirms the degradation of CrSBr when in air conditions. Therefore, in order to maintain the pristine state of the material when measuring its thermoelectric properties, the CrSBr flakes analyzed in this work have been encapsulated in hBN.

11 First principle simulations

We employ Density Functional Theory[16,17] as implemented in the ABINIT[18] software suite, in a projector augmented wave[19] basis using JTH[20] format atomic datasets with plane wave kinetic energy cutoffs of 25 and 30 Ha for the wavefunctions and density (total energies are converged to within 1 meV/atom). The first Brillouin Zone is sampled using a uniform grid of $13\times$ $9\times$ 3 points for the ground state and $26\times$ $18\times$ 6 to prepare transport calculations. The exchange correlation functional used was the generalized gradient approximation of Perdew Burke and Ernzerhof,[21] augmented by the Grimme D3 van der Waals dispersion.[22] The magnetism of Cr necessitates additional Hubbard repulsion in the DFT+U method[23] (Fully Localized Limit) with a U of 4 eV and J of 1 eV on Cr only (effective U of 3 eV). Most calculations are performed for collinear spins, and additional checks with non collinear magnetization and spin orbit coupling. The electronic bands are occupied with a Gaussian smearing of 10^{-4} Ha to improve convergence and allow for variable spin polarized occupations, though the final band structures are all semiconducting. The PM high temperature phase is approximated using the Special Quasirandom Structure (SQS) approach[24] implemented in the icet package[25] to generate spin configurations in the infinite temperature limit.[26] By averaging over 5 different $3\times3\times2$ supercells with these disordered spins configurations, we obtain a representative electronic DOS and states for the high temperature phase.

12 Evaluation of the transport coefficients

The transport coefficients are calculated within the constant relaxation time approximation using the Boltztrap2 code[?] for constant doping levels. The Seebeck coefficient is obtained quantitatively as the (unknown) relaxation time drops out of its expression. We infer the experimental doping level ($\sim 8\cdot10^{18}$ carriers per cm^3) by the best fit to the experimental $\alpha(T)$ at low temperature in the AFM phase. The doping is considered constant above T_N as well. This is a good approximation if T is high enough that all dopants are ionized, but not so high that new charge-donating defects are created. We also apply the Boltztrap2 code to the PM approximant SQS supercells, then the

results are averaged, in order to estimate the transport of the PM phase. To compare to the experimental transport measures, we add a crossover/switching from AFM to PM, inspired by Ref.[27] The switching is chosen as an error function (erf) centered at T_N with a width of 30 K.

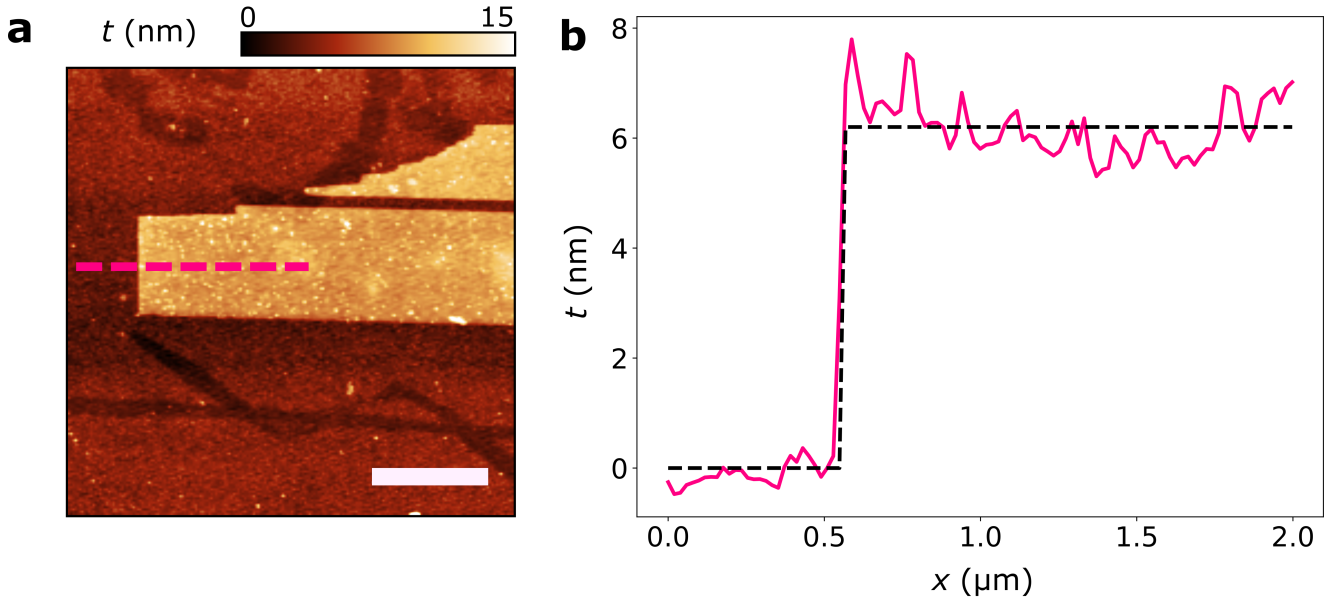

Fig. S 1. Atomic Force Microscopy image of the CrSBr flake. a) Topography of the flake. b) Thickness profile (in magenta) along the dashed line in (a). The average height of the flake is defined by the black dashed line. Scale bar: 1 μm.

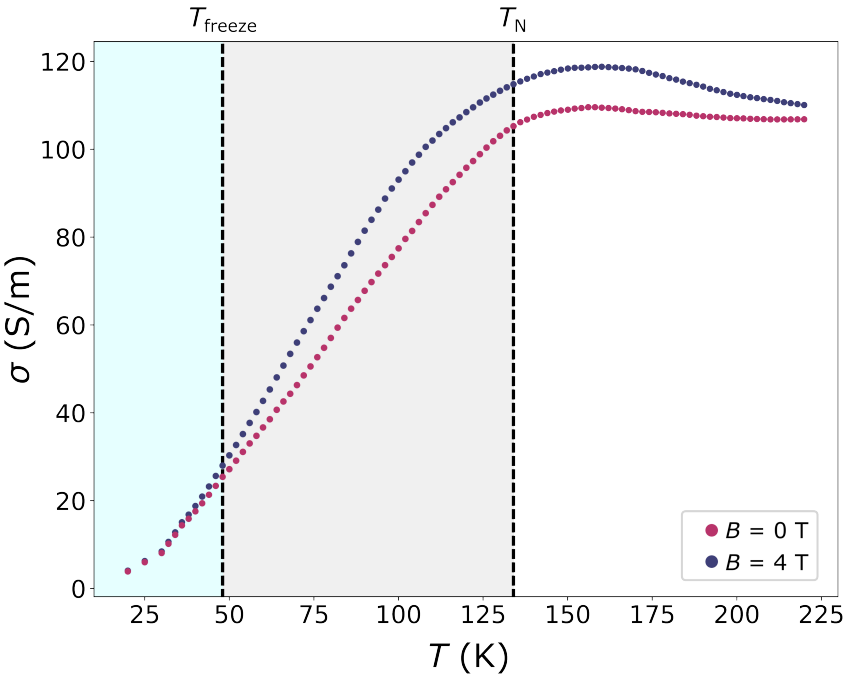

Fig. S 2. Temperature-dependent electrical conductivity σ of the CrSBr flake. σ is evaluated by measuring the conductance G with $B = 0$ T (purple curve) and $B = 4$ T (blue curve). The geometrical parameters are extrapolated via optical microscopy (l, w) and Atomic Force Microscopy (t). The characteristic temperatures T_N and T_{freeze} are reported on top of the graph. The white area is associated to the PM phase, while the grey/cyan one is associated to the AFM one.

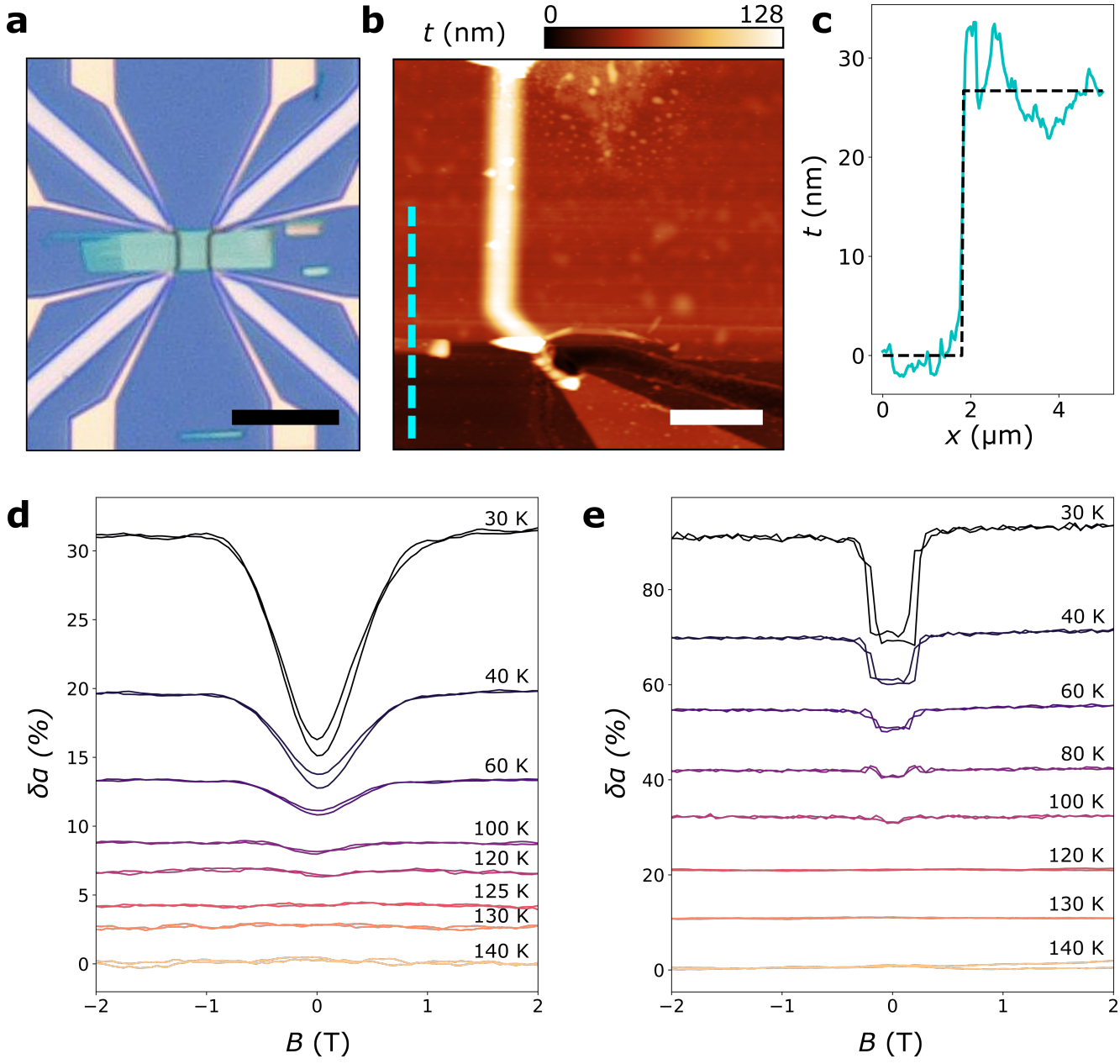

Fig. S 3. Additional field-dependent measurements of the thermoelectric properties of CrSBr. a) Optical image of the CrSBr device. Scale bar: 20 μm. b) Topography of the device measured via Atomic Force Microscopy. c) Thickness profile (in cyan) along the dashed line in (b). The average height of the flake is defined by the black dashed line. Scale bar: 2 μm. d,e) Magneto-Seebeck coefficient as a function of temperature, with external field B aligned with a axis (d) and b axis (e). Each curve is offset for clarity by 2% (d) and 10% (e) respectively.

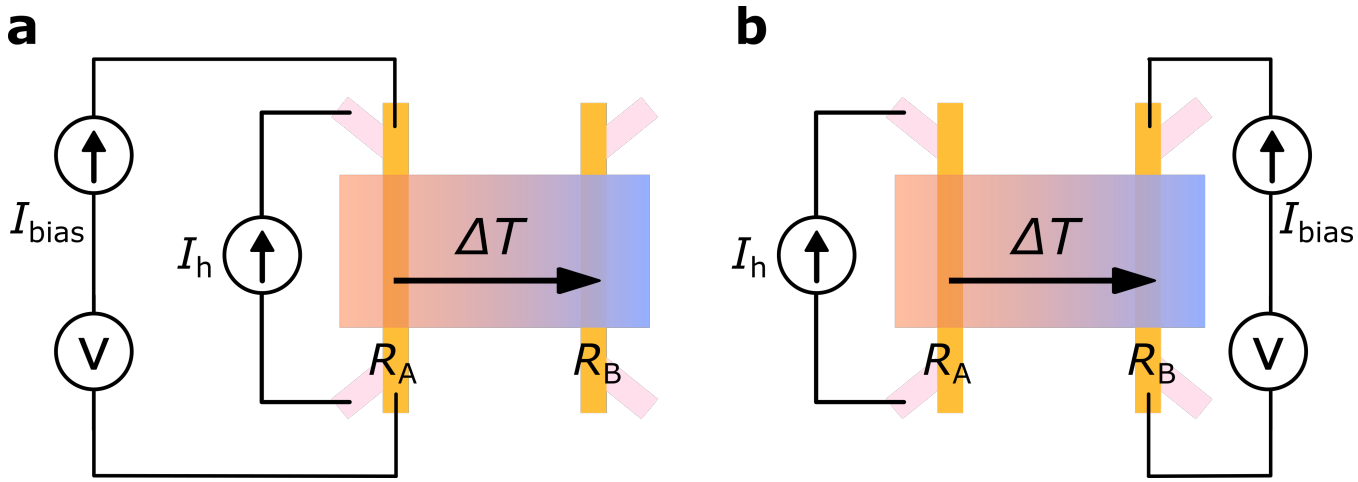

Fig. S 4. Measurement setup for the calibration of thermometers. A standard resistance measurement is performed on thermometer A (a) and B (b), while feeding the heater on a current I_h. The measurement is done with I_h=0 and then repeated with $I_h \neq 0$.

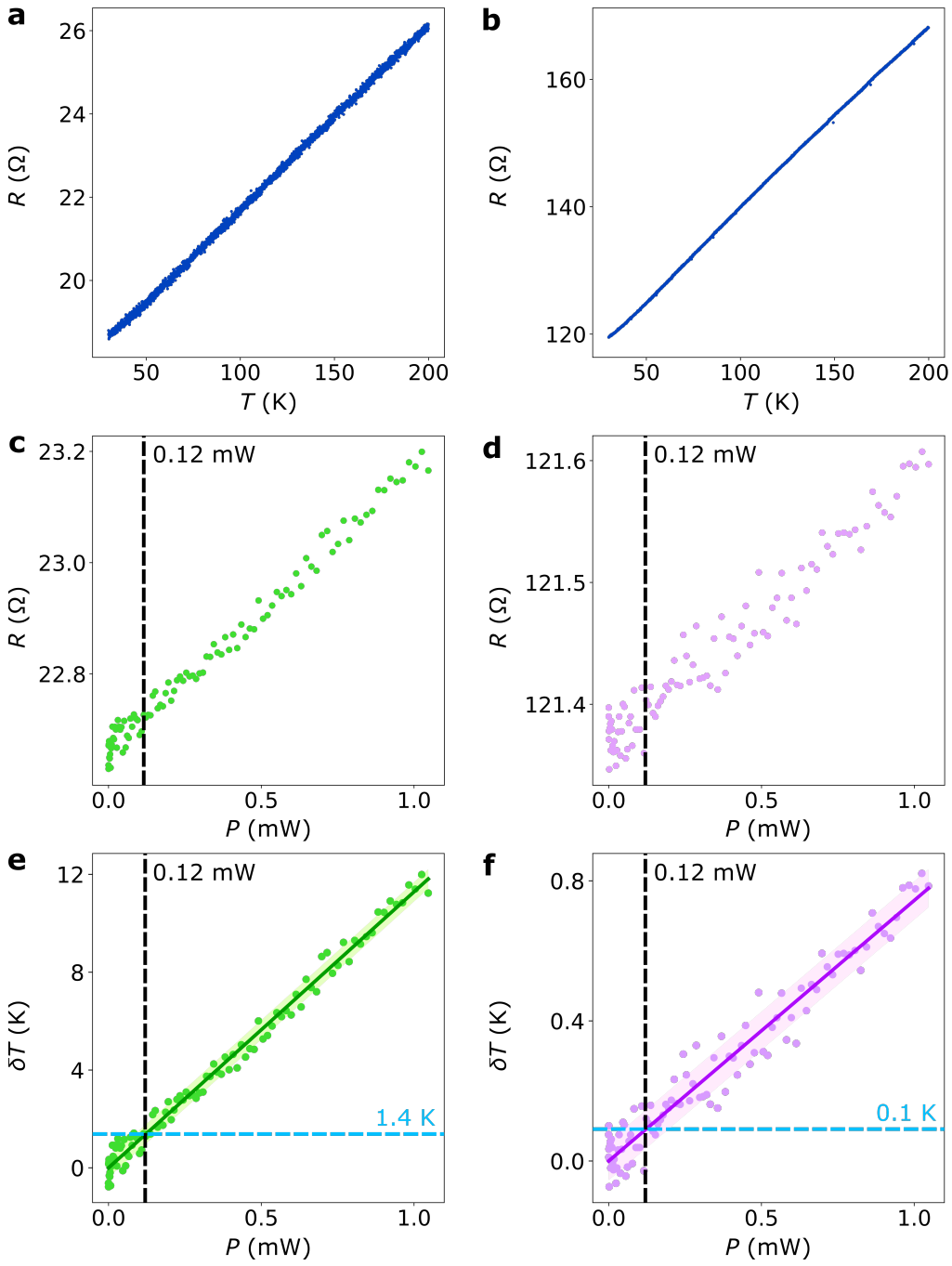

Fig. S 5. Calibration of the thermometers. a,b) Resistance of gold thermometers A (a) and B (b) vs T. c,d) Resistance of gold thermometers A (c) and B (d) as a function of the power P applied to the heater. e,f) Extracted temperature jump δT on thermometers A (e) and B (f) vs P. The black dashed line indicates the power value used in the experiments described in the main text (0.12 mW), while the cyan dashed line shows the corresponding temperature jump for the two thermometers (1.4 and 0.1 respectively).

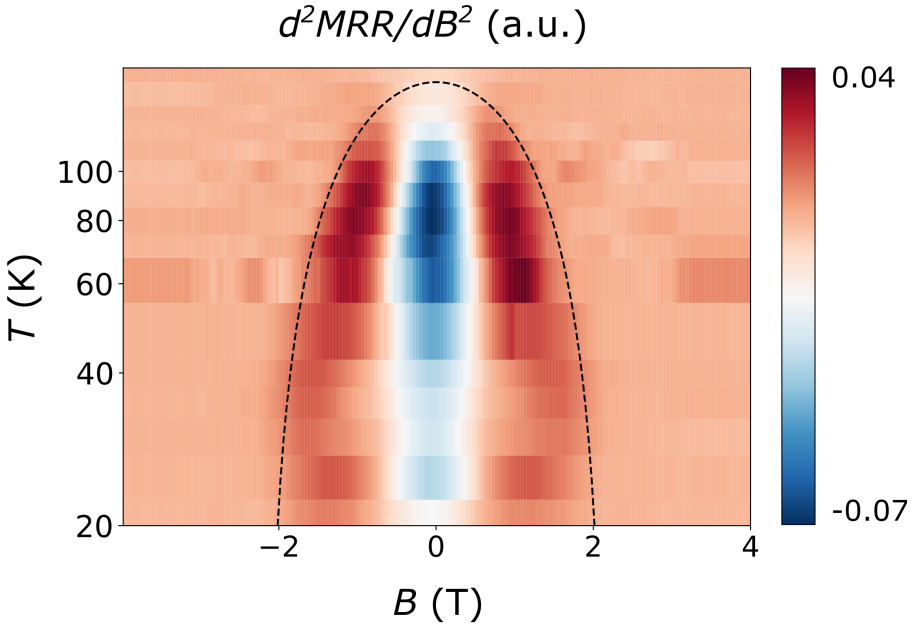

Fig. S 6. Evaluation of the saturation field. Colormap of the second derivative of the magnetoresistance ratio (MRR) versus temperature and applied magnetic field. The black dashed line defines the saturation field H_s.[9]

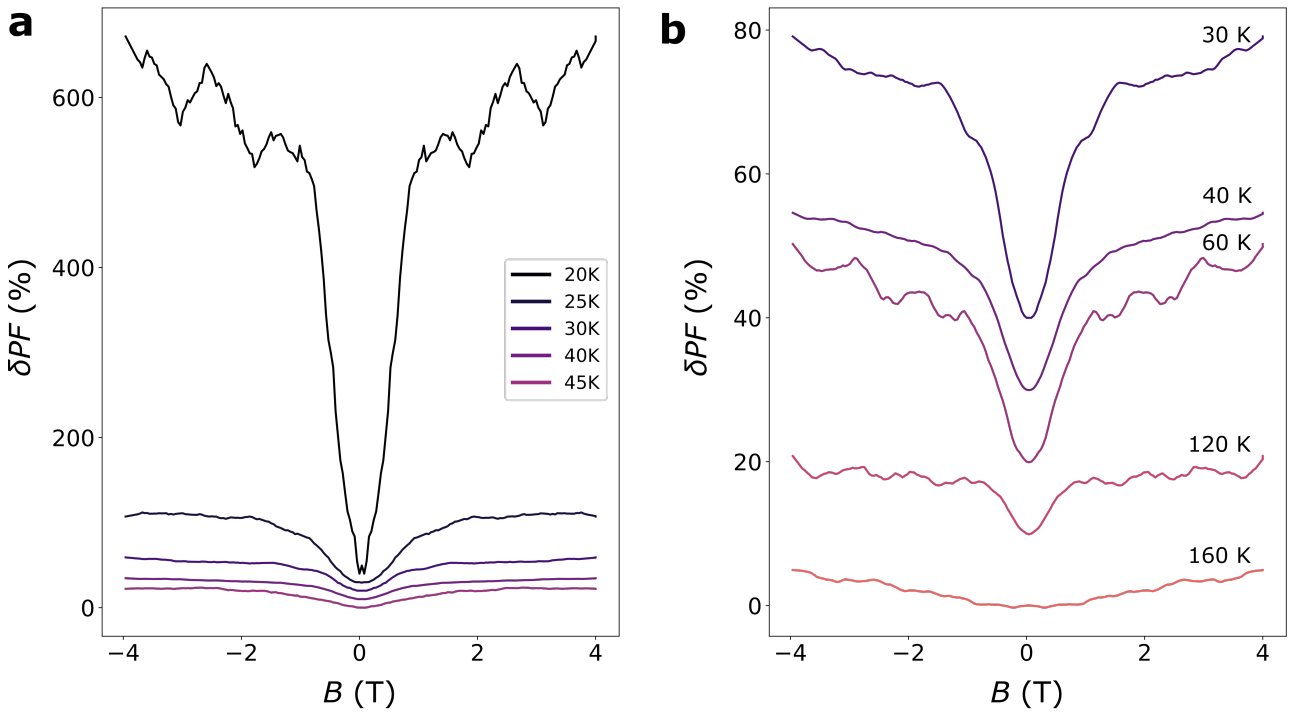

Fig. S 7. Field dependence of the magneto-power factor. The magneto-power factor is defined as $\frac{PF(B)-PF(0)}{PF(0)\cdot 100}$, where $PF = \alpha^2 \cdot \sigma$. Curves recorded at temperatures raging from 30 K to 160 K are reported in a), while b) shows in detail the curves between 20 K and 45 K.

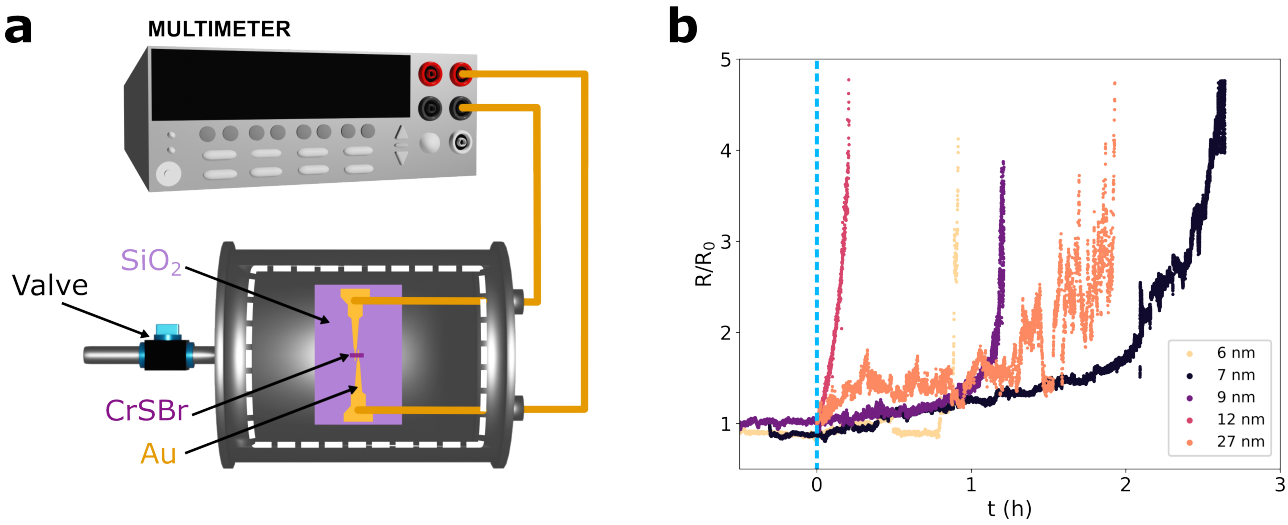

Fig. S 8. Degradation study of CrSBr flakes. a) Schematic of the measurement setup. The device is positioned in a home-made hermetically closed chamber equipped with a butterfly valve, which allows to first maintain the internal atmosphere of chamber inert and subsequently fill the chamber with air. b) Time-dependent resistance curves of CrSBr flakes with different thicknesses (see legend). At t = 0 (highlighted by a cyan dotted line), the valve is open and the chamber is filled with ambient air.

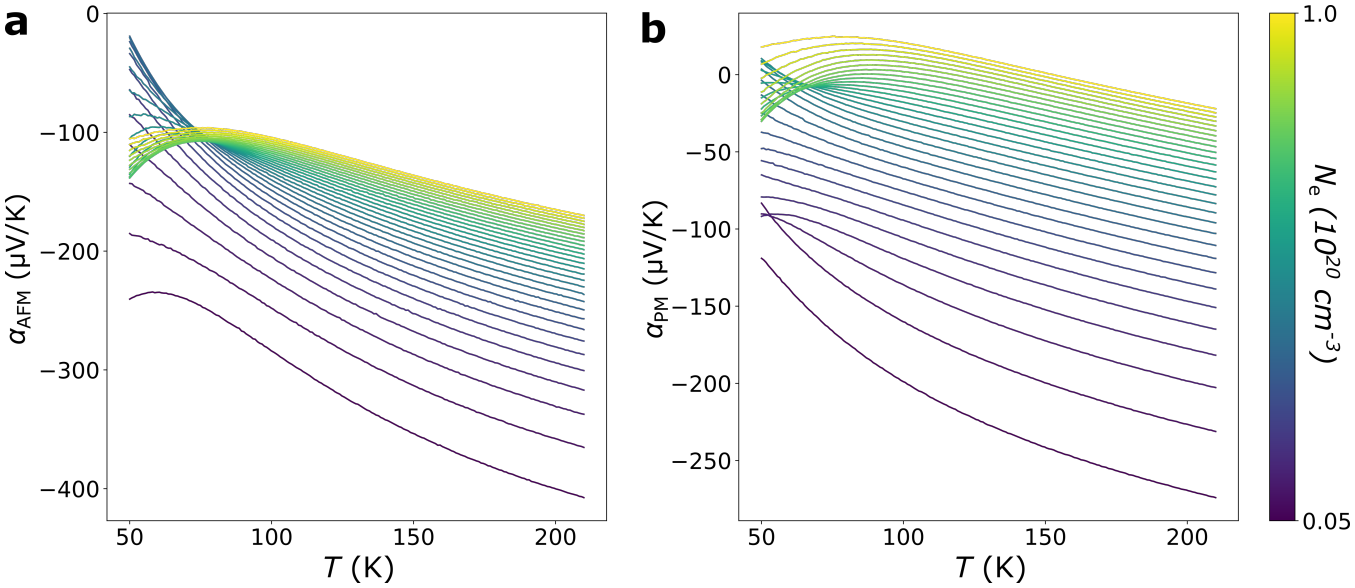

Fig. S 9. Temperature dependence of the Seebeck coefficient of CrSBr. Temperature-dependent variation of the Seebeck coefficient α at $B = 0$ T as a function of the doping concentration in the a) AFM state and b) PM state. The doping concentration values are reported in the colorbar on the right. With increasing doping, α amplitude decreases, and the values in the PM state are systematically smaller than in the AFM one. As discussed in the main text this is due to a smaller band gap and disorder effects on the electronic bands, which reduce their average dispersion and group velocity.

References

(1) Scheie, A.; Ziebel, M.; Chica, D. G.; Bae, Y. J.; Wang, X.; Kolesnikov, A. I.; Zhu, X.; Roy, X. Spin Waves and Magnetic Exchange Hamiltonian in CrSBr. *Advanced Science* **2022**, *9*, 2202467.

(2) Castellanos-Gomez, A.; Buscema, M.; Zant, H.; Steele, G. Deterministic transfer of two-dimensional materials by all-dry viscoelastic stamping. *2D Materials* **2013**, *1*, 011002.

(3) Frisenda, R.; Navarro-Moratalla, E.; Gant, P.; Perez de Lara, D.; Jarillo-Herrero, P.; Gorbachev, R.; Castellanos-Gomez, A. Recent progress in the assembly of nanodevices and van der Waals heterostructures by deterministic placement of 2D materials. *Chemical Society Reviews* **2017**, *47*, 53–68.

(4) Novoselov, K. S.; Geim, A. K.; Morozov, S. V.; Jiang, D.; Zhang, Y.; Dubonos, S. V.; Grigorieva, I. V.; Firsov, A. A. Electric Field Effect in Atomically Thin Carbon Films. *Science* **2004**, *306*, 666–669.

(5) Novoselov, K. S.; Jiang, D.; Schedin, F.; Booth, T. J.; Khotkevich, V. V.; Morozov, S. V.; Geim, A. K. Two-dimensional atomic crystals. *Proceedings of the National Academy of Sciences* **2005**, *102*, 10451–10453.

(6) Kinoshita, K.; Moriya, R.; Onodera, M.; Wakafuji, Y.; Masubuchi, S.; Watanabe, K.; Taniguchi, T.; Machida, T. Dry release transfer of graphene and few-layer h-BN by utilizing thermoplasticity of polypropylene carbonate. *npj 2D Materials and Applications* **2019**, *3*.

(7) Wang, L.; Meric, I.; Huang, P. Y.; Gao, Q.; Gao, Y.; Tran, H.; Taniguchi, T.; Watanabe, K.; Campos, L. M.; Muller, D. A.; Guo, J.; Kim, P.; Hone, J.; Shepard, K. L.; Dean, C. R. One-Dimensional Electrical Contact to a Two-Dimensional Material. *Science* **2013**, *342*, 614–617.

(8) Gehring, P.; Sowa, J.; Hsu, C.; Bruijckere, J.; Star, M.; Le Roy, J.; Bogani, L.; Gauger, E.; Zant, H. Complete mapping of the thermoelectric properties of a single molecule. *Nature Nanotechnology* **2021**, *16*, 1–5.

(9) Telford, E. J.; Dismukes, A. H.; Lee, K.; Cheng, M.; Wieteska, A.; Bartholomew, A. K.; Chen, Y.-S.; Xu, X.; Pasupathy, A. N.; Zhu, X.; Dean, C. R.; Roy, X. Layered Antiferromagnetism Induces Large Negative Magnetoresistance in the van der Waals Semiconductor CrSBr. *Advanced Materials* **2020**, *32*, 2003240.

(10) Lee, K.; Dismukes, A. H.; Telford, E. J.; Wiscons, R. A.; Wang, J.; Xu, X.; Nuckolls, C.; Dean, C. R.; Roy, X.; Zhu, X. Magnetic Order and Symmetry in the 2D Semiconductor CrSBr. *Nano Letters* **2021**, *21*, 3511–3517, PMID: 33856213.

(11) Ye, C.; Wang, C.; Wu, Q.; Liu, S.; Zhou, J.; Wang, G.; Söll, A.; Sofer, Z.; Yue, M.; Liu, X.; Tian, M.; Xiong, Q.; Ji, W.; Renshaw Wang, X. Layer-Dependent Interlayer Antiferromagnetic Spin Reorientation in Air-Stable Semiconductor CrSBr. *ACS Nano* **2022**, *16*, 11876–11883, PMID: 35588189.

(12) Liu, W.; Guo, X.; Schwartz, J.; Xie, H.; Dhale, N. U.; Sung, S. H.; Kondusamy, A. L. N.; Wang, X.; Zhao, H.; Berman, D.; Hovden, R.; Zhao, L.; Lv, B. A Three-Stage Magnetic Phase Transition Revealed in Ultrahigh-Quality van der Waals Bulk Magnet CrSBr. *ACS Nano* **2022**, *16*, 15917–15926, PMID: 36149801.

(13) Torres, K.; Kuc, A.; Maschio, L.; Pham, T.; Reidy, K.; Dekanovsky, L.; Sofer, Z.; Ross, F. M.; Klein, J. Probing Defects and Spin-Phonon Coupling in CrSBr via Resonant Raman Scattering. *Advanced Functional Materials* **2023**, *33*, 2211366.

(14) Telford, E. et al. Coupling between magnetic order and charge transport in a two-dimensional magnetic semiconductor. *Nature Materials* **2022**, *21*, 754–760.

(15) Ziebel, M. E.; Feuer, M. L.; Cox, J.; Zhu, X.; Dean, C. R.; Roy, X. CrSBr: An Air-Stable, Two-Dimensional Magnetic Semiconductor. *Nano Letters* **2024**, *0*, null, PMID: 38567828.

(16) Hohenberg, P.; Kohn, W. Inhomogeneous Electron Gas. *Phys. Rev.* **1964**, *136*, 864–871.

(17) Kohn, W.; Sham, L. J. Self-Consistent Equations Including Exchange and Correlation Effects. *Phys. Rev.* **1965**, *140*, A 1133 – A 1138.

(18) Gonze, X.; Amadon, B.; Antonius, G.; Arnardi, F.; Baguet, L.; Beuken, J.-M.; Bieder, J.; Bottin, F.; Bouchet, J.; Bousquet, E.; others The ABINIT project: Impact, environment and recent developments. *Computer Physics Communications* **2020**, *248*, 107042.

(19) Blöchl, P. E. Projector augmented-wave method. *Phys. Rev. B* **1994**, *50*, 17953–17979.

(20) Jollet, F.; Torrent, M.; Holzwarth, N. Generation of Projector Augmented-Wave atomic data: A 71 element validated table in the XML format. *Computer Physics Communications* **2014**, *185*, 1246–1254.

(21) Perdew, J. P.; Burke, K.; Ernzerhof, M. Generalized Gradient Approximation Made Simple. *Phys. Rev. Lett.* **1996**, *77*, 3865.

(22) Grimme, S.; Antony, J.; Ehrlich, S.; Krieg, H. A consistent and accurate ab initio parametrization of density functional dispersion correction (DFT-D) for the 94 elements H-Pu. *The Journal of Chemical Physics* **2010**, *132*, 154104.

(23) Anisimov, V.; Zaanen, J.; Andersen, O. Band theory and Mott insulators: Hubbard U instead of Stoner I. *Phys. Rev. B* **1991**, *44*, 943.

(24) Zunger, A.; Wei, S.-H.; Ferreira, L. G.; Bernard, J. E. Special quasirandom structures. *Physical Review Letters* **1990**, *65*, 353–356.

(25) Ångqvist, M.; Muñoz, W. A.; Rahm, J. M.; Fransson, E.; Durniak, C.; Rozyczko, P.; Rod, T. H.; Erhart, P. ICET – A Python Library for Constructing and Sampling Alloy Cluster Expansions. *Advanced Theory and Simulations* **2019**, *2*.

(26) Abrikosov, I.; Ponomareva, A.; Steneteg, P.; Barannikova, S.; Alling, B. Recent progress in simulations of the paramagnetic state of magnetic materials. *Current Opinion in Solid State and Materials Science* **2016**, *20*, 85–106.

(27) Körmann, F.; Grabowski, B.; Dutta, B.; Hickel, T.; Mauger, L.; Fultz, B.; Neugebauer, J. Temperature Dependent Magnon-Phonon Coupling in bcc Fe from Theory and Experiment. *Phys. Rev. Lett.* **2014**, *113*, 165503.